Transverse additive manufacturing and optical evaluation of miniature thin lenses in ultracompact micro multi-spherical compound eye

Xian Jing[a], Rongxin Zhu[a], Kaixuan Wang[a], Wenfang Si[a], Zhenyan Zhu[a], Xiuyuan Chen[b], Jieqiong Lin,[a,*] MingMing Lu[a]

[a] Provincial Key Laboratory of Micro/Nano and Ultra-precision Manufacturing, School of Mechatronic Engineering, Changchun University of Technology, Changchun 130012, China
[b] Centre for Precision Manufacturing, DMEM, University of Strathclyde, Glasgow, G1 1XQ, UK

E-mail: linjieqiong@ccut.edu.cn

Received xxxxxx
Accepted for publication xxxxxx
Published xxxxxx

Abstract

An ultracompact micro multi-spherical compound eye (MSCE) was designed to solve the defocus problem existing in traditional curved compound eye for planar photoelectric detection. The MSCE was integrated with a series of thin lenses located on multiple spherical surfaces with various radii. The overall diameter of the designed MSCE was 86.3μm, and it was composed of 37 ommatidia with a diameter of 7.5μm. The transverse additive manufacturing method via two-photon polymerization (TPP) was used to achieve precise fabrication of MSCE. Comparison experiments were performed to show the superiority of this method in quality and efficiency in thin lenses manufacturing compared with traditional curved compound eye methods. Furthermore, the spot diagrams and Modulation Transfer Function (MTF) curves were used to evaluate the optical imaging. The imaging of letters 'C', 'U' and 'T' through the fabricated MSCE were successfully detected by the established imaging system, respectively. The imaging quality was evaluated using the root-mean-square value in the Hexcone model. The maximum optical intensity of MSCE increased by 63.9% compared with that of a single-spherical compound eye (SSCE). Finally, the actual field of view (FOV) angle of MSCE was detected as ~80°, which was almost consistent with the theoretical angle of 77.6°. It is expected that this work will promote micro-optics components to be applied in the miniaturization and integration of optics systems for imaging, sensing and illuminating.

Keywords: compound eye, two-photon polymerization, additive manufacturing, optical evaluation, microfabrication

1. Introduction

Bio-compound eyes are the special visual organs formed during the long-term evolution of some nature creatures, such as insects, arthropods or bivalves in nature, which are composed of hundreds of integrated optical units called ommatidia[1, 2]. Their unique imaging mechanisms bring a lot of benefits for visual perception, such as highly effective performance, large FOV, rapid response and so on[3-5]. Inspired from their components, numerous artificial bionic compound eyes have been developed and widely used in pathological diagnosis[6], target tracking[7], intelligent camera [8-12], motion detection[13] and other significant fields. This indicates the rapid development of modern optics towards miniaturization, intelligence and integration.

So far, planar compound eyes and curved compound eyes have been proposed and designed by researchers[14-17]. The curved compound eye has attracted more attention due to the larger FOV and more similar structure to the natural compound eye than the planar compound eye. Various curved compound eyes have been developed and manufactured. For example, D. Wu et al. exploited a high-speed voxel-modulation laser scanning method to fabricate artificial compound eyes with full filling factor, large numerical aperture and free distortion [18]. However, the nonplanar arrangement of ommatidia on curved compound eyes brings a great challenge for its photoelectric detection, especially in the micro-optics field[19, 20]. Y. M. Song et al. [21] proposed a flexible detector for curved compound eye detection. But there are few curved photoelectric detectors that were totally matured to detect the imaging of curved compound eyes, especially in extra-small fields. Therefore, the planar photoelectric detector was used in most cases which led to a mismatch between the detection plane and imaging focal surface. Only several levels of ommatidia can be detected at a certain focal depth. Some solutions have been proposed to deal with the above problems. For example, Z. C. Ma et al. developed a smart artificial compound eye using stimuli-responsive proteins to achieve the tunable focal distance of ommatidia[22]. Other solutions including refractive lens array[23, 24], self-writing waveguide[25], optical fiber guidance[26], introduction prism [27], etc. However, all these solutions need additional external environments or components, which cause some fabrication challenges and system complexities.

TPP is one of the feasible ways which equipped with flexible 3D manufacturing capacity and nanoscale resolution in terms of achieving the manufacturing of micro compound eye among the various artificial compound eye processing. However, its traditional bottom-to-top additive method still has difficulties in dealing with the precision fabrication of thin lenses in the micro compound eyes. A large number of slicing layers are still needed to fit the thin lenses contours to meet the precision requirement, which will lead to an expatiatory program and low efficiency. The adaptive slicing method is a feasible way to reduce the number of layers, but it doesn't have obvious effects on micro-thin lenses[28, 29]. Furthermore, to evaluate the imaging quality of the micro compound eyes, the optical evaluation of miniature thin lenses array is still a crucial limitation [30]. Various methods are verified feasibly to evaluate the optical property of the compound eye on the macro scale. For example, the USAF test target is a representative method to assess resolution[31, 32]. Nevertheless, the optical evaluation of compound eye in micro-scale is still needed to be further explored due to its small size, low imaging quality and serious diffraction.

In the present work, a kind of MSCE was designed and fabricated via two-photon polymerization. It can realize all the ommatidia synchronously focused on a planar photoelectric detector with a single-layer compound eye without additional adjustable components. The transverse additive manufacturing method was proposed to fabricate MSCE and then compared with the traditional method. Meanwhile, the optical performance of the designed structure was investigated by the radius RMS values in terms of defocused spots and MTF curves. Imaging comparison experiments involved a series of letters through the single-spherical compound eye (SSCE) and MSCE were conducted to assess the imaging performance, respectively. Lightness value in the Hexcone model was used to evaluate the light intensity in the images. Finally, the actual FOV angle of MSCE was measured to make a comparison with the theoretical value.

2. Theory

Normally, the ommatidia of SSCE are arranged on a spheric surface. Fig. 1(a) shows the ray tracing of incident light illuminating on a SSCE. There will be a mismatch between the SSCE focal spots and the planar photoelectric detector. Then, the structure parameters of a SSCE are demonstrated in Fig. 1(b). It is obvious that the ommatidia arrays are distributed symmetrically in a ring and were numbered as 0, 1, 2, 3-level from the center to the periphery as shown in Fig. 1(a), respectively.

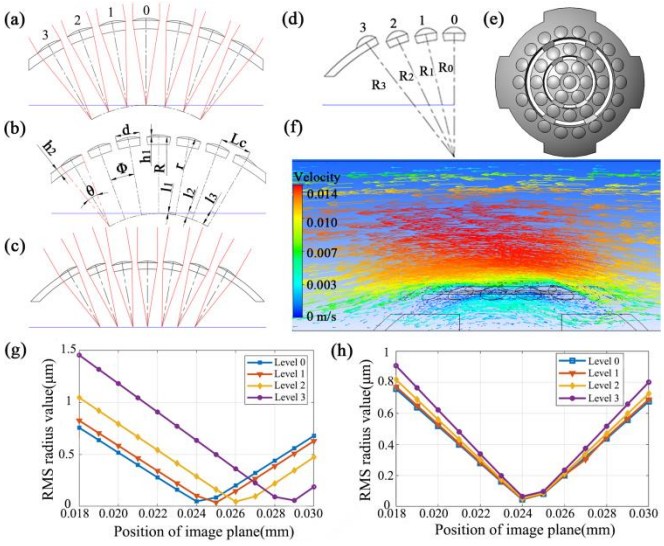

Fig. 1. Design of MSCE. (a) Ray tracing of a SSCE. (b) Sectional view of a single-spherical compound eye. (c) Ray tracing for MSCE. (d) The radii of 0, 1, 2, 3-level ommatidia in MSCE. (e) Top view of a MSCE. (f) Flow simulation of developer around MSCE. (g) RMS radius values of spot diagrams in SSCE versus different imaging distances. (h) RMS radius values of spot diagrams in MSCE versus different imaging distances.

The diameters of natural compound eyes range from a few microns to tens of microns in most cases. In this paper, the diameters of ommatidia *d* in SSCE were selected 7.5 μm. To

simplify the processing, the curvature radii of ommatidia r were designed to be 10μm to confine the overall height of the compound eye within the working distance range of objective. Likewise, the curvature radius of substrate R was chosen to be 54.4μm. The thickness of the substrate h_2 was designed to be 2.4μm according to the experientially support thickness.

According to the thin lenses manufacturing equation, the focal length f of each ommatidium can be calculated by Eq. 1.

$$\frac{1}{f}=(n-1)\left(\frac{1}{r}-\frac{1}{R}\right) \tag{1}$$

Where n is the refractive index of the photoresist.

The defocus distance l_N of each ommatidium can be obtained by Eq. 2.

$$l_N=\frac{R-f}{\cos(N\Phi)}+f-R \tag{2}$$

Where N is the level of ommatidium. The defocus distances of 1, 2, 3-level ommatidium were 0.461μm, 1.919μm, 4.626μm, respectively.

Angular resolution of ommatidia is one of the important parameters effecting the FOV. It refers to the angle between adjacent ommatidia, which can be obtained from Eq. 3.

$$\Phi=2\arcsin(L_C/2R) \tag{3}$$

Where L_c is the distance between two adjacent ommatidia on the outer surface of the substrate, which is 9.48μm.

The FOV angle θ of an individual ommatidium can be obtained from Eq. 4.

$$\theta=2\arcsin(d/2f) \tag{4}$$

The overall FOV angle Ψ of compound eye can be calculated by the Eq. 5 (Here Ψ=77.6°).

.

$$\Psi=\theta+2(N-1)\Phi \tag{5}$$

Unlike the single-spherical substrate surface of SSCE, the ommatidia of MSCE considering different levels were located at four spheric surfaces with various curvature radii as shown in Fig. 1(c). The distances between each level of ommatidia and photoelectric detection plane are determined by the optimal imaging distances. The substrates with different level are placed on concentric circles with various radii. The curvature radius of substrate is R_N, as shown in Fig. 1(d). (N is the level of ommatidium). Thus, R_N can be calculated by Eq. 6.

$$R_N=\frac{R_0-f}{\cos(N\Phi)}+f \tag{6}$$

After calculation, we can obtain R_0=54.4μm, R_1=54.86μm, R_2=56.32μm, R_3= 59.03μm, respectively. Obviously, the radii of 1, 2, 3-level spherical substrate in MSCE were increased compared with SSCE. Thus, the 1, 2, 3-level ommatidia were expanded outward along optical axes. Besides, the fabricated compound eye was formed on the glass substrate within the photoresist. The polymerized compound eye structure and glass substrate would generate a confined space if there is no channel. The unpolymerized photoresist inside the compound eye should be dissolved by developer. Therefore, supports and gaps were considered to improve the development of unpolymerized photoresist as shown in Fig. 1(e). Meanwhile, the hydrodynamic simulation was conducted to predict the development state around MSCE in the fluid developer. According to the actual development process, the average flow rate was set as 10mm/s. Fig. 1(f) demonstrates the fluid flow around MSCE. The flow rate of developer inside the MSCE was improved from 0 mm/s to ~3mm/s due to the designed supports and gaps. It is sufficient to dissolve the unpolymerized photoresist inside the fabricated structure during a short time. Otherwise, low surface quality and undesired structure will be generated during the post-processing in the case of the residue of unpolymerized photoresist can't be removed completely. This method provides an effective way to improve the developing efficiency and surface quality of MSCE.

Fig. 1(g) and Fig. 1(h) show the RMS radius values of focal spots of SSME and MSCE varying with the imaging distances of ommatidia, respectively. The spot RMS values of 0, 1, 2, 3-level ommatidia in SSCE reach minimum at different imaging distances while the corresponding values in MSCE reach minimum at a same imaging distance. It is concluded that MSCE is more suitable for planar photodetection than SSCE in theory. The minimum spot RMS values of every level ommatidium in MSCE were not showed in Fig. 1(h) as the decimal place limitation of the simulation software.

Fig. 2(a-d) figure the spot diagrams of ommatidia at different levels, respectively. The spot RMS radius values of 0, 1, 2, 3-level ommatidia are 0.049μm, 0.051μm, 0.056μm and 0.068μm, respectively.

The diameter of airy disk r_s can be obtained by Eq. 7.

$$r_s=2.44*F*\lambda \tag{7}$$

Where λ is the dominant wavelength. The value of F is 5.43, which is the reciprocal of the relative aperture. Thus, the radius of the airy spot is 7.78μm by the above calculation. It is clearly seeing that all the spot radii of ommatidia are less than r_s which indicates that the ommatidia of MSCE meet the requirements of optical system.

Fig. 2(e) shows the MTF curves considering different levels of MSCE structure at tangential direction and Fig. 2(f-i) demonstrate them at sagittal direction. MTF is the modulus of Optical Transfer Function (OTF) and it has been widely adopted to describe the optical properties of system. MTF curve explains the contrast of the images at different spatial frequencies. The cutoff frequency is the limiting frequency, which indicates the optical resolution of lens. And the cutoff frequency of the MSCE can be calculated through Eq. 8.

$$v=\frac{1}{\lambda*F} \tag{8}$$

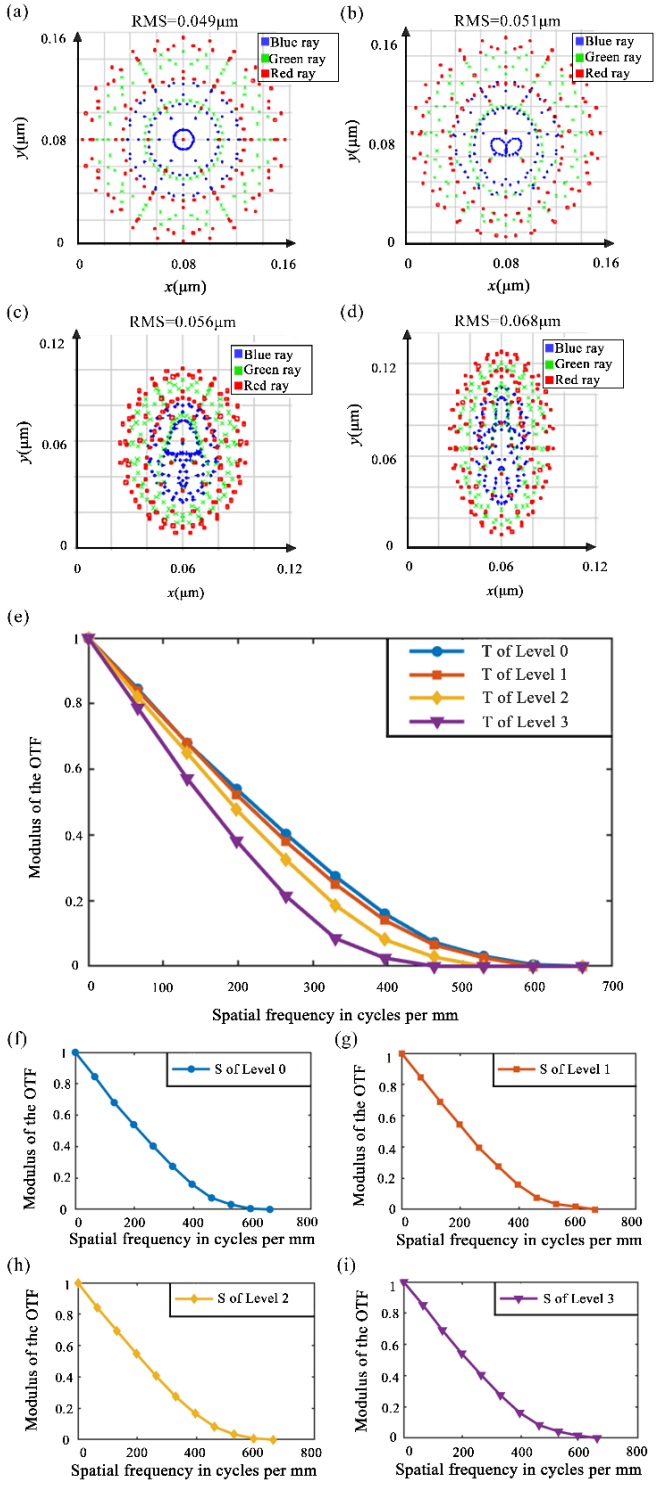

Fig. 2. (a-d) Spot diagrams of 0, 1, 2, 3-level ommatidia. (e) Tangential MTF curves of 0, 1, 2, 3-level ommatidia. (f-i) Sagittal MTF curves of 0, 1, 2, 3-level ommatidia, respectively.

Obviously, the 3-level ommatidia demonstrate the worst performance of all the ommatidia. Thus, if the parameters of 3-level ommatidia can achieve standard, the others will meet the related requirements. Besides, the cutoff frequency of 3-level ommatidia is 313 lp/mm which theoretically given by Eq. 8. The simulated cutoff frequency of 3-level ommatidia is 469 lp/mm and 594 lp/mm on the tangential plane and on the sagittal plane, respectively, as shown in Fig. 2(e) and Fig. 2(i). As conclusion, all the simulated cutoff frequencies were greater than theorical value. And the points which needed to be attached more attention are the MTF value is greater than 0.3 and the curve is smooth when the spatial frequency is 220 lp/mm, which indicates the ommatidium fill the need of imaging[33].

3. Results and discussion

Ormocer, a kind of organic modified ceramics, was used as the photoresist in this work. And it was evenly spin-coated on the substrate and then pre-baked at 90℃ for 10 minutes. In the experiment, a titanium-sapphire mode-locked oscillator with a wavelength of 800nm, a pulse width of 100fs and a repetition frequency of 80MHz were used to induce TPP. Commercially available OrmoDev® was applied to construct the target structures.

The designed MSCE was fabricated by TPP as shown in Fig. 3. And the structure was divided into three parts, including inner contour, outer contour and infill. It was constructed with additive manufacturing method by scanning laser focal spot layer by layer. Fig. 3(a) shows the fabrication schematic diagram of MSCE. Meanwhile, Fig. 3(b) and Fig. 3(c) demonstrate the manufacturing path of a hemispheroid in traditional vertical and transverse additive manufacturing methods, respectively. Fig. 3(d-g) claim the simulated hemispheroids with layer thicknesses L_{th} of 2μm, 1μm, 0.2μm and 0.1μm, respectively. These figures show that low slope region in the top of the hemispheroid improve little with the reduction in layer thickness. Meanwhile, it can be assured that the ommatidia in the compound eye are exactly thin lenses with low slopes, which causes a large number of layers and low efficiency. Although transverse additive manufacturing method seems similar with traditional vertical additive method in some aspects, they possess an essential difference in dealing with thin lens. It is common realized that low slope has no obvious effect on the surface quality in transverse additive manufacturing method. However, this method was not be widely used in popular macro additive manufacturing such as Fused Deposition Modeling(FDM), Stereo Lithography Apparatus(SLA), Selective Laser Sintering(SLS) and so on. It is because that this method needs a vertical manufacturing. And the vertical direction-oriented processing may induce movement interference between nozzle and adjacent fabricated structure or materials padding difficulty. However, it is feasible for TPP. TPP only forms structure at focal spot region and has no limitation about fabricating directions and padding. All these factors make transverse additive manufacturing succeed in the application. Fig. 3(h) and Fig.3(i) show the SEM images of fabricated MSCEs with a layer thickness of 0.13μm by vertical additive manufacturing and

transverse additive manufacturing, respectively. The laser power is 34 mW and scanning speed is 25μm/s. Long-stroke air-bearing linear stages with 1 nm positioning resolution used as positioning devices to lay the foundation of prospective large-scaling and high-efficiency manufacturing for future industrial production. The relatively low position accuracy of linear stage compared with micropositioner is also equipped with the benefit to verify the superiority of the proposed methods. Fig. 3(j) and Fig.3(k) show the partial enlarged detail of central region used vertical additive manufacturing method and transverse additive manufacturing method, respectively.

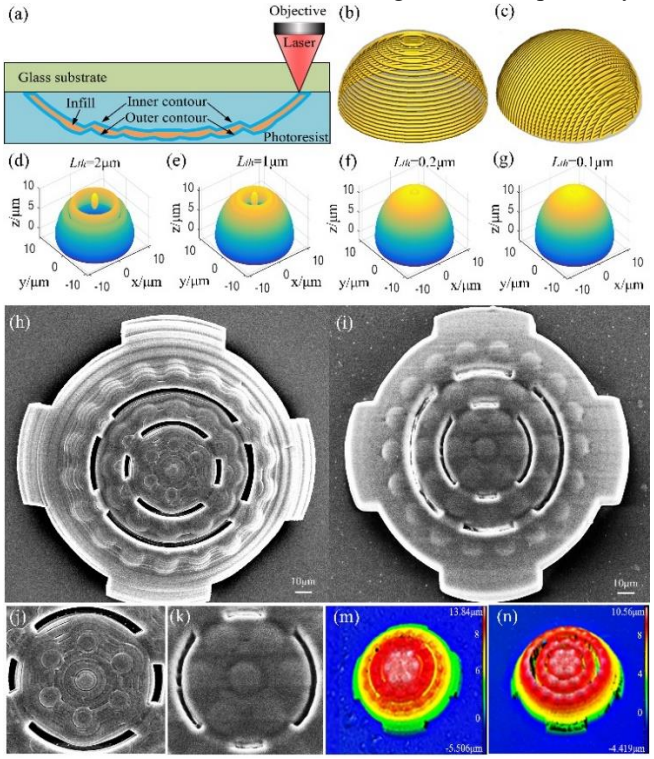

Fig. 3. Fabrication of compound eyes. (a) Schematic diagram of MSCE fabrication. (b) Vertical fabrication path of a hemispheroid. (c) Transverse fabrication path of a hemispheroid. (d-g) simulated hemispheroids with layer thicknesses L_{th} of 2μm, 1μm, 0.2μm and 0.1μm, respectively. (h) SEM image of the MSCE fabricated with vertical method. (i) SEM image of the MSCE fabricated with transverse method. (j) Partial enlarged detail of central region with vertical method. (k) Partial enlarged detail of central region with transverse method. (m) Surface topography of overall SSCE. (n) Surface topography of overall MSCE.

Compared with the conspicuous microgrooves caused by ladder errors in vertical additive manufacturing method, a relative smooth surface was obtained in the MSCE using transverse additive manufacturing method. Besides, a SSCE was designed and fabricated to compare with the designed MSCE in the aspect of the optical performance. The surface topography of SSCE and MSCE were detected by optical profiler as shown in Fig. 3(m) and Fig. 3(n), respectively. The images show that the fabricated MSCE has a good surface quality and the appearance is consistent with the targeted structure.

In this paragraph, an imaging system was constructed to detect the fabricated micro compound eyes as shown in Fig. 4(a). The schematic diagram of imaging system was shown in Fig. 4(b). It consisted of a bromine-tungsten lamp, computer, 3D positioning stage, objective lens and CCD camera. And the prepared compound eye sample was placed on the 3D micromotion stage in the imaging experiment. The position of the compound eye sample was fine-tuned by this stage to facilitate imaging at the CCD camera. The computer was used to show the imaging results. And a photomask with T-shape through-hole was placed on a holder between the light source and compound eye.

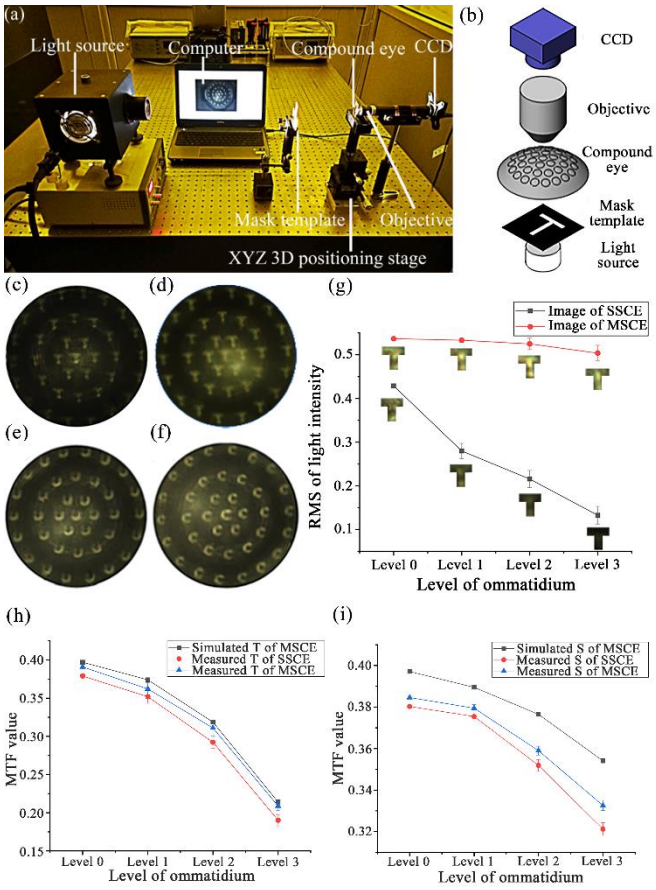

Fig. 4. Imaging detection of Compound eye. (a) Compound eye imaging system. (b) Schematic diagram of imaging system. (c) Imaging of 'T' through SSCE. (d) Imaging of 'T' through MSCE. (e) Imaging of 'U' through MSCE. (f) Imaging of 'C' through MSCE. (g) Light intensity RMS of 'T' imaging. (h) The simulated and measured tangential MTF value of SSCE and MSCE. (i) The simulated and measured sagittal MTF value of SSCE and MSCE.

It can be clearly seen that both SSCE and MSCE were detected by the imaging system. The imaging images of letter 'T' through the SSCE and MSCE were shown in Fig. 4(c) and Fig. 4(d), respectively. Hexcone model is a kind of colour space proposed by A. R. Smith to describe the image. It is also

called HSV model where 'H', 'S' and 'V' represented hue, saturation and value, respectively. The values in Hexcone model were used to evaluate the light intensity of detecting image. To avoid noise and disturbance, only the light intensity in T-shape imaging region was considered. Accordingly, the RMS values of light intensity in the T-shape region were used to evaluate the imaging quality of SSCE and MSCE.

The RMS value curves of light intensity at various levels are shown in Fig. 4(g). As shown in the Fig. 4(g), the light intensity distribution of the traditional SSCE decays from 0-level to 3-level gradually while that of MSCE shows a relatively good uniformity. The optical intensities of 1, 2, 3-level ommatidia increased by 34.1%, 48.5%, 63.9%, respectively. Furthermore, the imaging experiments of letters 'U' and 'C' through MSCE were also conducted to verify the applicability of MSCE for other type images, respectively. The images of 'U' and 'C' are showed in Fig. 4(e) and Fig. 4(f), respectively.

These results verify the proposed MSCE successfully in terms of solving the defocus problem existing in SSCE. The horizontal and vertical lines of 'T' photomask were used as one line pair test, which aims to measure the MTF value. And the nonopaque part is acted as the white line and its adjacently opaque part of photomask is served as the black line. The nonuniform illumination of light source is subtracted. Last but not least, the tangential and sagittal MTF value of imaging image at a spatial frequency of 267 lp/mm was measured and compared with the simulated results, as shown in Fig. 4(h) and Fig. 4(i), respectively.

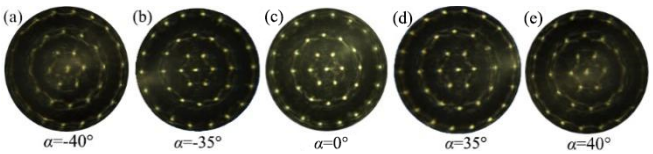

Fig. 5. Measurement of FOV angle. The incident angle of MSCE ranged from -40° to 40°

According to the discussions above, the experimental MTF value decreases from 0-level to 3-level ommatidium gently which makes agreement with the tendency of simulated results. And this phenomenon is caused by the orientations of the ommatidia deviate from illumination optical axis from 0-level to 3-level gradually. Besides, the MTF value of MSCE show an almost negligible difference with that of SSCE because their ommatidia are different in position but same in orientation and structural parameters. The difference between experimental and simulated MTF values can be explained by the surface difference between the actual fabricated compound eye and ideal compound eye. The results claim that MSCE improves the imaging quality mainly from the lightness instead of MTF value. Nevertheless, MTF curves remain an effective basis to evaluate the optical property of compound eye in structural design stage.

The FOV can be served as a crucial parameter to assess compound eye performance. Fig. 5 shows imaging results of spots under different incident angles ranging from -40° to 40°. When the absolute value of incident angle was less than or equal to 35°, the light intensity of every ommatidia shows a good uniformity. But when the absolute value of incident angle was 40°, the light intensity of ommatidia was partially disappeared on one side. That means the actual FOV angle of MSCE is ~80°, which is consistent with the theoretical FOV angle 77.6°.

4. Conclusion

In general, a kind of ultra-compact micro MSCE was designed and fabricated by two-photon polymerization technology to solve the defocusing problem existing in traditional SSCE for planar photoelectric detection. A transverse additive manufacturing method was proposed to improve the surface quality of thin lenses in the compound eyes. Its superiority is experimentally compared with the traditional vertical additive manufacturing method. The spot diagrams and MTF curves were utilized to evaluate the optical property of the designed MSCE. The images of letters 'C', 'U' and 'T' were successfully detected by the established MSCE imaging system, respectively. The imaging of MSCE was compared with that of traditional SSCE. The results showed MSCE has a more uniform optical intensity. Especially, the optical intensity at the outer edge increased by 63.9%. It is expected that this work will promote micro-optics component to be applied in the miniaturization and integration of optics systems for imaging, sensing and illumination.

Acknowledgements

The authors acknowledge support from the Department of Science and Technology of Jilin Province (20140622008JC, 20190201303JC).

Declaration of Competing Interest

The authors declare no conflicts of interest.

References

[1] Jeong KH, Kim J, Lee LP. Biologically inspired artificial compound eyes. Science 2006; 312(5773): 557-561.
[2] Elwell M, Wen L. The power of compound eyes. Optics & Photonics News 1991; 9(2): 100-103.
[3] Lei L, Yi AY. Development of a 3D artificial compound eye. Opt. Express 2010; 18(17): 18125-18137.
[4] Lee L, Szema R. Inspirations from Biological Optics for Advanced Photonic Systems. Science 2005; 310(18): 1148-1150.
[5] Wei K, Zeng H, Zhao Y. Insect-human hybrid eye (IHHE): an adaptive optofluidic lens combining the structural characteristics of insect and human eyes. Lab on a Chip 2014; 14(18): 3594-3602.

[6] Lee GJ, Choi C, Kim DH, Song YM. Bioinspired artificial eyes: optic components, digital cameras, and visual prostheses. Adv. Funct. Mater 2017; 28(24): 1705202.1-1705202.17.

[7] Colonnier F, Manecy A, Juston R, Mallot H, Leitel R, Floreano D, Viollet S. A small-scale hyperacute compound eye featuring active eye tremor: application to visual stabilization, target tracking, and short-range odometry. Bioinspir. Biomim 2015; 10(12): 026002 .

[8] Shi CY, Wang YY, Liu CY, Wang TS, Zhang HX, Liao WX, Xu ZJ, Yu WX. SCECam: a spherical compound eye camera for fast location and recognition of objects at a large field of view. Opt. Express 2017; 25(26): 32333.

[9] Liang WL, Pan JG, Su J, Guo D. One-lens camera using a biologically based artificial compound eye with multiple focal lengths. Optica 2019; 6(3): 326-334.

[10] Ko HC, Stoykovich MP, Song JZ, Viktor M, Choi WM, Yu CJ, Joseph BG, Xiao JL, Wang SD, Huang YG, John AR. A hemispherical electronic eye camera based on compressible silicon optoelectronics. Nature 2008; 454(7205): 748-753.

[11] Yu XD, Liu CY, Zhang YJ, Xu HR, Wang YY, Yu WX. Multispectral curved compound eye camera. Opt. Express 2020; 28(7): 9216-9231.

[12] Xu HR, Zhang YJ, Wu DS, Zhang G, Wang ZY, Feng XP, Hu BL, Yu WX. Biomimetic curved compound-eye camera with a high resolution for the detection of distant moving objects. Opt. Lett 2020; 45: 6863-6866.

[13] Zhang BS, Chen G, Cheng MC, Chen JM, Zhao Y. Motion detection based on 3D-printed compound eyes. OSA Continuum 2020; 45(24): 2553-2563.

[14] Zhang H, Li L, Mccray DL, Scheiding S, Naples NJ, Gebhandrt A, Risse S, Eberhardt R, Tünnermann A, and Yi AY. Development of a low cost high precision three-layer 3D artificial compound eye. Opt. Express 2013; 21(19): 22232-22245.

[15] Tian ZN, Yao WG, Xu JJ, Yu YH, Chen QD, Sun HB. Focal varying microlens array. Opt. Lett 2015; 40(18): 4222-4225.

[16] Zheng YL, Song L, Huang JX, Zhang HY, Fang FZ. Detection of the three-dimensional trajectory of an object based on a curved bionic compound eye. Opt. Lett 2019; 44(17): 4143-4146.

[17] Li J, Wang WJ, Mei XS, Pan AF, Sun XF, Liu B, Cui JL. Artificial Compound Eyes Prepared by a Combination of Air-Assisted Deformation, Modified Laser Swelling, and Controlled Crystal Growth. ACS Nano2019; 13(1): 114-124.

[18] Wu D, Wang JN, Niu LG, Zhang XL, Wu SZ, Chen QD, Lee LP, Sun HB. Bioinspired Fabrication of High-Quality 3D Artificial Compound Eyes by Voxel-Modulation Femtosecond Laser Writing for Distortion-Free Wide-Field-of-View Imaging. Adv. Opt. Mater 2014; 2(8): 751-758.

[19] Chung T, Lee YS, Yang SP, Kim K, Kang BH, Jeong KH. Mining the smartness of insect ultrastructures for advanced imaging and illumination. Adv. Func. Mater 2018; 28(24): 1705912.

[20] Deng HX, Gao XC, Ma MC, Li YY, Li H, Zhang J, Zhong X. Catadioptric planar compound eye with large field of view. Opt. Express 2018; 26(10): 12455-12468.

[21] Song YM, Xie YZ, Viktor M, Xiao JL, Jung I, Choi KJ, Liu ZJ, Park HS, Lu CF, Kim RH, Li R, Crozier KB, Huang YG, John AR. Digital cameras with designs inspired by the arthropod eye. Nature 2013; 497(7447): 95-99.

[22] Ma ZC, Hu XY, Zhang YL, Liu XQ, Hou ZS, Niu LG, Zhu L, Han B, Chen QD, Sun HB. Smart Compound Eyes Enable Tunable Imaging. Adv. Funct. Mater 2019; 29(38): 1903340.

[23] Lei L, Yi AY. Design and fabrication of a freeform microlens array for a compact large-field-of-view compound-eye camera. Appl. Opt 2012; 51(12): 1843-1852.

[24] Jing X, Wang KX, Zhu RX, Lin JQ, Yu BJ, Lu MM. Design and Fabrication of Double-Layer Curved Compound Eye via Two-Photon Polymerization. IEEE Photonic. Tech. L. 2021; 33(5): 231-234.

[25] Kim J, Jeong KH, Lee LP. Artificial ommatidia by self-aligned microlenses and waveguides. Opt. Lett 2005; 30(1): 5-7.

[26] Liu F, Yang Q, Bian H, Zhang F, Hou X, Kong DP, Chen F. Artificial compound eye-tipped optical fiber for wide field illumination. Opt. Lett 2019; 44(24); 5961-5964.

[27] Ma MC, Guo F, Cao ZL, Wang KY. Development of an artificial compound eye system for three-dimensional object detection. Appl. Opt. 2014; 53(6): 1166-1172.

[28] Guo R, Xiao SZ, Zhai XM, Li JW, Xia D, Huang WH. Micro lens fabrication by means of femtosecond two photon photopolymerization. Opt. Express 2006; 14(2): 810-816.

[29] Jing X, Wang KX, Lin JQ, Liu P, Kan YD, Zheng X, Sun J, Li YC. Adaptive Slicing Method for Three-Dimensional Microstructures with Free-Form Surfaces in Two Photon Polymerization Microfabrication. Nano 2019; 14(1): 1950006.

[30] Tanida J, Kumagai T, Yamada K, Miyatake S, Ishida K, Morimoto T, Kondou N, Miyazaki D, Ichioka Y. Thin observation module by bound optics (TOMBO): concept and experimental verification. Appl. Optics 2001; 40(11): 1806-1813.

[31] Brückner A, Duparré J, Leitel R, Dannberg P, Tünnermann A. Thin wafer-level camera lenses inspired by insect compound eyes. Opt. Express 2010; 28(24): 24379.

[32] Ma MC, Zhang Y, Deng HX, Gao XC, Gu L, Sun QZ, Su YL, Zhong X. Super-resolution and super-robust single-pixel superposition compound eye. Opt. Laser. Eng. 2021; 146: 106699.

[33] Pang K, Fang FZ, Le S, Zhang Y, Zhang HY. Bionic compound eye for 3D motion detection using an optical freeform surface. Journal of the Optical Society of America B Optical Physics 2017; 34(5): B28.